Published in final edited form as:

J Immunol. 2019 August 15; 203(4): 899–910. doi:10.4049/jimmunol.1801649.

Kynurenine 3-monooxygenase inhibition during acute SIV infection lowers PD-1 expression and improves post-cART CD4+ T cell counts and body weight:

KMO inhibition improves clinical outcome in SIV infection

Louise A. Swainson[1], **Haelee Ahn**[1], **Priya Pajanirassa**[1,*], **Vinod Khetarpal**[2], **Claire Deleage**[3], **Jacob D. Estes**[3,#], **Peter W. Hunt**[1], **Ignacio Munoz-Sanjuan**[2], **Joseph M. McCune**[1,+]

[1]Division of Experimental Medicine, UCSF, San Francisco, CA, USA

[2]CHDI Management/CHDI Foundation, Los Angeles, CA, USA

[3]AIDS and Cancer Virus Program, Frederick National Laboratory for Cancer Research, Leidos Biomedical Research, Inc., Frederick, MD, USA

Abstract

The kynurenine pathway (KP) is a key regulator of many important physiological processes and plays a harmful role in cancer, many neurological conditions, and chronic viral infections. In HIV infection, KP activity is consistently associated with reduced CD4 T cell counts, and elevated levels of T cell activation and viral load (VL); it also independently predicts mortality and morbidity from non-AIDS events. Kynurenine 3-monooxygenase (KMO) is a therapeutically important target in the KP. Using the non-human primate model of simian immunodeficiency virus (SIV) infection in rhesus macaques, we investigated whether KMO inhibition could slow the course of disease progression. We utilized a KMO inhibitor (KMOi), CHDI-340246, to perturb the KP during early acute infection and followed the animals for one year to assess clinical outcomes and immune phenotype and function during pre-cART acute infection and cART-treated chronic infection. Inhibition of KMO in acute SIV infection disrupted the KP and prevented SIV-induced increases in downstream metabolites, improving clinical outcome as measured by both increased CD4+ T cell counts and body weight. KMO inhibition increased naïve T cell frequency and lowered PD-1 expression in naïve and memory T cell subsets. Importantly, early PD-1 expression during acute SIV infection predicted clinical outcomes of body weight and CD4+ T cell counts. Our data indicate that KMO inhibition in early acute SIV infection provides clinical benefit, and suggest a rationale for testing KMO inhibition as adjunctive treatment in SIV/HIV infection to slow progression of disease and improve immune reconstitution.

*Current affiliation: Intellia Therapeutics, Cambridge, MA, USA

#Current affiliation: Vaccine and Gene Therapy Institute and Oregon National Primate Research Center (ONPRC), Oregon Health and Science University (OHSU), Oregon, USA.

+Current affiliation: Innovative Technology Solutions, The Bill & Melinda Gates Foundation, Seattle, WA, USA

Introduction

Progressive HIV disease is marked by systemic inflammation and immune dysregulation, most notably CD4+ T cell depletion (1–4). The persistence of immune activation, even in long-term cART-treated individuals, is associated with increased risk of AIDS and non-AIDS morbidities, including cardiovascular disease, cancers, and modulated neurocognition (5, 6). Several factors have been identified as associated with immune dysfunction and disease progression; for example, KP metabolites and the increased expression of inhibitory molecules like PD-1 (7–11).

The KP is the principal pathway by which tryptophan (TRP) is metabolized, and is a key regulator of many important physiological processes such as energy production, protein synthesis, immune response, and excitatory neurotransmission (12–15). The rate-limiting step of the KP is the conversion of TRP to kynurenine (KYN) by IDO, which is inducible by inflammatory stimuli. KYN is usually hydroxylated to 3-hydroxy kynurenine (3HK) by kynurenine 3-monooxygenase (KMO) and then further converted to 3-hydroxy anthranilic acid (3HAA). 3HAA is rapidly converted to quinolinic acid (QA), and proceeds with conversion to NAD+, a preferred end product of the KP (13).

Many studies have shed light on the role of the KP, suggesting that it plays a harmful role in cancer, many neurological conditions, and chronic viral infections such as HIV (10, 16). Monocyte-derived dendritic cells (DCs)expressing IDO promote regulatory T cell (Treg) expansion (17). KP metabolites can also act as aryl hydrocarbon receptor (AhR) ligands, which allow the generation of Treg cells (18). In addition, several KP metabolites inhibit T cell proliferation directly, further contributing to a hyperinflammatory state (19), while QA damages brain tissue leading to dementia (20). We and others have shown that IDO and KMO activity leads to loss of Th17 cells, which play an important role in maintaining the gut mucosal epithelial barrier (9, 10, 21–23). This reduction in Th17 cells was found to be mediated by 3HAA, a downstream metabolite of KYN and KMO activity (10), and can result in microbial translocation and systemic inflammation (24).

In HIV infection, IDO activity, is consistently linked to reduced CD4 T cell counts, and elevated levels of T cell activation and VL (11, 25). In addition, the KYN/TRP ratio independently predicts mortality and morbidity from non-AIDS events (5, 6, 25, 26). The KP has also been implicated in the pathogenesis of HIV associated neurocognitive disorder (HAND); for example, neurotoxic QA is elevated in the cerebrospinal fluid of patients with AIDS dementia (20, 27).

KMO is a therapeutically important target in the KP (28–31), where it converts KYN to 3HK. Inhibition of this enzyme shifts the flux in the pathway towards the formation of neuroprotectant kynurenic acid (KYNA), and away from the ROS-generating and toxic metabolites, 3HK and QA (29). Notably, KMO expression is higher in pro-inflammatory than in anti-inflammatory macrophages (32), and increases in inflammatory conditions or after immune stimulation (33).

Based on the extensive research indicating that the KP is detrimental in HIV infection, we investigated whether KMO inhibition could impact the course of HIV disease progression

utilizing a well-established model of SIV infection in rhesus macaques. We utilized a KMOi, CHDI-340246, to perturb the KP during the first 4 weeks of infection (a period during acute infection when KP activity is a key discriminator between pathogenic and non-pathogenic SIV infection (9)) and followed the animals for one year to assess clinical and immunological outcomes during pre-cART acute infection and cART-treated chronic infection. Our data indicate that such KMO inhibition provides clinical benefit in SIV infection, and suggest a rationale for testing KMO inhibition as adjunctive treatment in SIV/HIV infection.

Materials and Methods

Study design

16 male rhesus macaques of 4–5 years of age were intravenously challenged with SIVmac251 after testing negative for SRV, STLV, hepatitis B, and helminthic infections. The viral stock was previously characterized and obtained from Nancy Miller (NIH). 8 animals received KMOi CHDI-340246 (10 mg/kg) daily via oral gavage, and the other 8 control animals received vehicle only for 4 weeks, commencing the day prior to SIV infection. Peripheral blood was sampled to evaluate the pharmacokinetics and pharmacodynamics (PK/PD) of CHDI-340246, VL, CD4+ T cell counts, immune phenotype and function, and microbial translocation. Rectal pinch biopsies (RB) and peripheral lymph node (LN) biopsies were taken to understand the impact of KMO inhibition on tissue immune phenotype and function. The study design and schedule is shown in Fig 1.

After the 4 week treatment period with CHDI-340246, animals were followed for an additional 50 weeks post infection (p.i.). At 14 weeks p.i., animals commenced a cART treatment regimen of once daily subcutaneous injections of tenofovir (TFV, Gilead), 20 mg/kg, emtricitabine (FTC, Gilead), 40 mg/kg, and dolutegravir (DTG, ViiV), 2.5 mg/kg until study completion at 54 weeks p.i. All protocols were approved before implementation by the Institutional Animal Care and Use Committee at Bioqual, Inc. Health, food intake, and body weights were recorded regularly according to established protocols.

Phenotypic analysis of lymphocyte populations

Thawed PBMCs were surface stained with Aqua amine reactive viability dye (Invitrogen) and mAbs to CD45 (clone D058–1283, BD Biosciences), CD3 (clone SP34–2, BD Biosciences), CD4 (clone L200, BD Biosciences), CD8 (clone 3B5, Invitrogen), CD95 (clone DX2, BioLegend), CD28 (clone CD28.2, Beckman), CD127 (clone hIL-7R-M21, BD Biosciences), PD-1 (clone EH12.2H7, BioLegend), and HLA-DR (clone L243, BD Biosciences) for 20 min at room temperature, fixed, and then permeabilized with FoxP3 Fix/Perm Buffers (eBioscience) per the manufacturer's instructions. Permeabilized cells were then stained intracellularly for Ki67 (clone B56, BD Biosciences) and FoxP3 (clone PCH101, eBioscience) for 30 min at 4°C, washed in FoxP3 Perm/Wash buffer, fixed in 0.5% paraformaldehyde and analyzed by flow cytometry on a BD LSRII flow cytometer (BD Biosciences) and analyzed using Flowjo Software (Tree Star Inc).

Cytokine Flow Cytometry (CFC)

Analysis of IL-2, IL-17, IL-4, IFNα, and TNFα production in PMA/ionomycin or p27 (Gag) peptide stimulated CD4+ or CD8+ T cells was carried out by cytokine flow cytometry, as previously described (34). Fixed and permeabilized cells were analyzed by flow cytometry on a BD LSRII flow cytometer (BD Biosciences) and analyzed using Flowjo Software (Tree Star Inc).

ELISAs

Plasma was stored at −80°C prior to analysis. Cytokines were measured using ELISA kits for sCD14 (R&D Systems), IP-10 (R&D Systems), sTNFRα1 (R&D Systems), and IL-7 (R&D Systems), according to the manufacturers' instructions.μ

Quantification of KMOi CHDI-340246 in plasma

Determination of CHDI-340246 in monkey plasma was performed using a liquid chomatography-tandem mass spectrometry (LC/MS/MS) method. A 25 μL aliquot of plasma was mixed with 200 μL of methanol:acetonitrile (50:50; v:v) containing CHDI-340246-d3 (100 ng/mL) as internal standard followed by centrifugation for 5 min at 3000 rcf. A 50 μL aliquot of supernatant was removed and mixed with 300 μL of 0.1% ammonium hydroxide in water at 1000 rcf for 1 min and then held at 4°C until analyzed by HPLC/MS. The supernatant was analyzed by injecting 10 μL onto an Agilent Pursuit XRs C18 (2.0 × 50 mm, 3 μm) column maintained at 40°C. The mobile phase flow rate was 0.7 mL/min and initial conditions comprised of 50% 10 mM ammonium bicarbonate and 0.4% ammonium hydroxide in water (mobile phase A) and 50% 10 mM ammonium bicarbonate and 0.4% hydroxide in methanol:water (90:10; v/v)(mobile phase B). The separation of CHDI-340246 was achieved using a gradient that increased from 50% mobile phase B at time 0 to 80% mobile phase B at 1.7 min with initial conditions returning at 2 min. The mass spectrometer used was API 4000 with TurboSpray in positive ionization mode. The transition ions (m/z) monitored were 291.1 → 218.0 for CHDI-340246 and 296.1 → 223.0 for CHDI-340246-d3 (the ^{37}Cl isotope of the internal standard was monitored to avoid contribution from the analyte). The calibration standard range was 10 ng/mL to 10,000 ng/mL and the lower limit of quantitation (LLOQ) was 10 ng/mL. CHDI-340246 was found to be stable in plasma following storage at −20°C up to 3 months and following freeze/thaw cycle.

Quantification of KP metabolites in plasma

Determination of KP metabolites in plasma were determined using 3 separate LC/MS/MS methods. A 5-analyte method was used for simultaneous analysis of KYN, KYNA, 3HK, AA and 3HAA. A second method was used for analysis of QA and a third method was employed to quantitate TRP in plasma. The stability of KP metabolites in plasma following storage at −20°C up to 3 months and following freeze-thaw cycle was established prior to analysis of the samples. For the 5-analyte method, a 200 μL aliquot of plasma was first mixed with 25 μL of 10% ascorbic acid followed by addition of 50 μL of internal standard solution (acetonitrile:water; 50:50) containing KYN-D6 (100 ng/mL), KYNA-D5 (50 ng/mL), $^{15}N^{13}C_2$ 3HK (100 ng/mL), and $^{13}C_6$ AA (50 ng/mL). To this mixture, 800 μL of acetonitrile/methanol (90:10; v:v) was added to precipitate the proteins. After mixing and

centrifugation, a 700 μL aliquot of supernatant was transferred to a clean tube and evaporated at 40°C for up to 2 h using TurboVap. The dried extract was then reconstituted with 100 μL of 0.1% formic acid in water. The separation of analytes was achieved by injecting 25 μL of reconstituted extract on a Waters XSelect HSS T3 (2.1 × 50 mm, 2.5 μm) column maintained at ambient temperature. The mobile phase (flow rate - 0.4 mL/min) was comprised of 0.1% formic acid in HPLC grade water (mobile phase A) and 100% acetonitrile (mobile phase B) with 0% B at initial conditions (time 0) and gradient starting at 0.1 min and reaching up to 95% B at 3.8 min, which was then maintained up to 4.3 min. Using API 5000 mass spectrometer with MRM scan mode and Turbospray ionization in positive mode, the transition ions monitored were as follows: KYN, 290.2 → 94.0; KYNA, 190.0 → 162.0; 3-HK, 225.1 → 162.1; AA, 138.0 → 92.0; 3-HAA, 154.0 → 108.0; KYN-D6, 215.2 → 98.0; KYNA-D5, 195.0 → 167.0; $^{15}N^{13}C_2$ 3-HK, 228.1 → 163.1, and $^{13}C_6$ AA, 144.1 → 98.0. The calibration ranges were 200 ng/mL to 160,000 ng/mL for KYN, 2.0 to 1600 ng/mL for KYNA and 3-HK, 5.0 to 4000 ng/mL for AA, and 20.0 to 16000 ng/mL for 3-HAA. The LLOQ was 200, 2.0, 2.0, 5.0, and 20.0 ng/mL for KYN, KYNA, 3-HK, AA, and 3-HAA, respectively.

For analysis of QA in plasma, a 30 μL aliquot was mixed with 30 μL of internal standard solution containing QA-D3 (250 ng/mL) followed by addition of 120 μL of methanol:pyridine (80:20; v:v). The mixture was centrifuged at 3000 rcf at 4°C for 10 min and a 100 μL of supernatant was transferred to a clean tube and mixed with 45 μL of 0.5M NaOH and then centrifuged. QA and internal standard were derivatized by adding 20 μL of methyl chloroformate and then mixing for 10 min at 500 rpm. Following mixing, 600 μL of 2% formic acid was added and the sample was centrifuged at ~3000 rcf for 5 min. The supernatant was injected on an Ascentis Express Phenyl-Hexyl (3 × 75 mm, 2.7 μm) column maintained at 40°C. The mobile phase flow rate was 0.45 mL/min and comprised of 5 mM ammonium formate /acetonitrile (85:15)(mobile phase A) and acetonitrile (mobile phase B) with initial conditions set at 4% mobile phase B and maintained up to 3.0 min, changing to 100% at 3.10 min and then reversing back to 4% B at 3.7 min. The mass spectrometer used was API 5000 with TurboSpray and in positive ionization mode. The transition ions monitored were 194.4 → 164.2 for QA and 199.4 → 167.2 for QA-D3. The calibration standard range was 20 ng/mL to 20,000 ng/mL and the LLOQ was 20 ng/mL.

For analysis of TRP in plasma, a 25 μL aliquot was mixed with 400 μL of internal standard solution (acetonitrile/methanol; 90:10) containing TRP-D5 (5000 ng/mL). Following mixing for 1 min at 1000 rpm, the samples were centrifuged at 3000 rcf for 5 min. A 50 μL of supernatant was transferred to a clean tube containing 800 μL of 0.1% formic acid. The supernatant was analyzed by injection on a Waters Xbridge C18 (2.1 × 50 mm, 2.5 μm) column maintained at 40°C. The mobile phase flow rate was 0.4 mL/min and comprised of 0.1% formic acid in water (mobile phase A) and 0.1% in acetonitrile (mobile phase B). The initial conditions were 5%B which increased to 30%B from 0.3 min to 1.2 min and then to 98% at 1.3 min which were maintained up to 1.8 min and then returning to initial conditions at 1.9 min. Using an API 4000 mass spectrometer, with TurboSpray in positive ionization mode, the transition ions monitored were 205.1 → 146.1 for TRP and 210.1 → 150.0 for TRP-D5. The calibration standards range was 500 ng/mL to 500,000 ng/mL and the lower limit of quantitation (LLOQ) was 500 ng/mL.

For all methods described above, each run was monitored by including quality controls (QCs) at 4 levels (low, low-mid, mid, and high) and acceptability of the concentration data for each analyte was based on ±15% CV for all QCs, except for low QC where acceptability was based on ±20% CV.

Immunohistochemistry (IHC) and in situ hybridization (ISH)

IHC, ISH and quantitative image analysis was performed for collagen, MPO, TGFβ and IL-17 on RB and inguinal LN samples, as previously described (35–39). IL-17 (A83173, Sigma), MPO (A0398, DAKO), and TGFβ (sc-146-G, Santa Cruz) IHC staining were performed on formalin-fixed, paraffin-embedded LN and/or RB tissue of 5 μm sections; collagen deposition was evaluated using Picro Sirius Red and light green staining. Entire tissue sections were scanned at high magnification (×200) using the ScanScope AT2 System (Aperio Technologies), then representative regions of interest (500 × 500 μm) were identified and high-resolution images extracted. The % area of each positive staining was quantified using Cell Profiler.

Statistical analysis

Differences between treatment groups in the change from baseline were assessed with linear mixed models (STATA 14.2), transforming outcome variables as appropriate to satisfy model assumptions. Timepoint by treatment group interaction terms were used to assess whether the change from baseline at each timepoint differed by treatment group. When more than one pre-SIV infection timepoint was available for a given analyte, all values contributed to each animal's baseline estimate to improve precision. When consistent trends were evident across multiple timepoints, post-hoc analyses were conducted to assess the significance of those trends across all timepoints. Significance was defined as $P < 0.05$. For the PK/PD data, differences between treatment groups at indicated timepoints was assessed using Wilcoxon rank sum analysis.

Results

Study Design

To determine whether inhibition of KMO might have an impact on acute SIV infection, 16 rhesus macaques were infected i.v. with SIVmac251. 8 animals were treated for 4 weeks with 10 mg/kg/day of the KMOi, CHDI-340246, and 8 animals served as vehicle only controls, starting the day prior to infection. Between 12 and 14 weeks p.i., 3 animals (2 controls and 1 KMOi-treated animal) were euthanized due to AIDS-related symptoms. At 14 weeks p.i., all remaining animals were placed on cART until study completion at 54 weeks p.i. In addition to PK/PD evaluation and monitoring of VL and CD4+ T cell counts, measures of immune phenotype and function were collected from peripheral blood, inguinal LN, and RB at the timepoints indicated in Fig. 1.

KMO inhibition increases CD4+ T cell counts and body weight in SIV-infected animals

To establish whether KMO inhibition has an impact on clinical outcomes in SIV infection, peripheral blood CD4+ T cell counts, body weight, and plasma RNA VL were measured (Figs. 2A, B, and C). After cART initiation, CD4+ T cell counts between the groups

diverged and KMOi-treated animals demonstrated significantly higher CD4+ T cell counts at 32 and 52 weeks p.i (Fig. 2A). A consistent increase in CD4+ T cell counts across all timepoints was apparent during cART in the KMOi-treated group. This trend was formally tested using linear mixed models, with KMOi-treated animals experiencing a mean 29 cell/mm^3 greater CD4+ T cell count increase than placebo-treated animals across all timepoints after cART initiation (P=0.033).

The juvenile macaques used in this study exhibited continued growth despite SIV infection, as expected. Body weight increased equivalently in both treatment groups until 7 weeks after cART initiation, when growth trends diverged (Fig. 2B.). These trends became more pronounced over time, with KMOi-treated animals exhibiting significantly greater weight gain than the vehicle-treated controls at almost all timepoints after 28 weeks p.i. By the end of the study, KMOi-treated animals had gained double the weight of the controls (+45% of baseline weight vs. +22% of baseline weight, respectively).

No significant differences were observed in plasma RNA VL between treatment groups at any timepoint ($P > 0.05$) (Fig. 2C). The time to achieve undetectable virus (< 50 copies/ml) was highly variable and dependent on set point VL rather than treatment status. At 36 weeks p.i. (22 weeks after cART initiation), undetectable VL was achieved in 10/13 animals, with occasional ‘blipping’ occurring in some animals. Two animals retained VL of 10^4 - 10^5 copies/ml until 44 weeks p.i. when darunavir (800 mg/day) was supplemented to their cART regimen. Notably, these animals had the highest VL pre-cART (7×10^8 and 3×10^9 copies/ml), despite higher than average CD4+ T cell counts.

KMOi CHDI-340246 disrupts the KP and prevents SIV-induced increases in downstream metabolites

To determine the PK of CHDI-340246, drug levels were measured in plasma by LC/MS/MS. Cmax reached 96 μM after first dose, with Tmax of 2.5 h, and a drug half-life of 6.3 h (Fig. 3B). Of note, there were no significant differences in PK parameters between the first and the last dose, indicating that drug clearance mechanisms were not affected by the treatment itself (Fig. 3B).

To understand the impact of KMOi administration on KMO activity, plasma concentrations of TRP, KYN, its KMO-catalyzed metabolite 3HK, KYN-level alternative branch metabolites anthanilic acid (AA) and kynurenic acid (KYNA), and the 3HK downstream metabolite QA were measured by LC/MS/MS (Fig. 3C). CHDI-340246 is highly selective for KMO vs other enzymes in the kynurenine pathway (40). Effective inhibition of KMO activity should increase the concentration of KYN, AA and KYNA, and decrease the concentration of 3HK and QA, leaving TRP levels unchanged. (Fig. 3A). These patterns were indeed observed, with CHDI-340246-treated animals reaching KYN, KYNA, and AA Cmax of 1–2 orders of magnitude higher than the control animals, and 3HK and QA concentrations in treated animals dropping to approximately one third the levels present in control animals (Fig. 3C).

Fig. 3D shows trough plasma concentrations of KYN and QA thoughout the first 56 days, during which animals were dosed daily with either KMOi CHDI-340246 or vehicle for the

first 28 days. As expected, SIV infection in the control group induced increased concentrations of both KYN and QA, peaking at 11 days p.i. The disruptive effect of KMO inhibition on the KYN pathway was to increase the KYN levels above that in the control group after infection and to completely inhibit any increase in QA levels above baseline levels thoughout the dosing period (Fig. 3D). At 42 days p.i., metabolite levels in both groups were equivalent, indicating complete drug wash out by 2 weeks after the end of dosing.

The KMOi CHDI-340246 was safe at the treatment dose used in this study. Complete blood count and extensive chemistry tests were performed to evaluate, e.g., RBC, WBC, hemoglobin, platelets, liver and kidney function, electrolytes and minerals (data not shown). In addition, animals were monitored closely for any abnormal clinical signs or behavior. No toxicities or safety concerns arose in the KMOi-treated animals.

KMO inhibition lowers PD-1 expression in CD4+ and CD8+ T cells of SIV-infected animals

The KP pathway has been implicated in altering immune activation and clinical outcomes in HIV/SIV infection (9, 10, 21, 22). To determine whether KMOi treatment inhibited T cell activation, expression levels of PD-1, HLA-DR, and cell cycle marker Ki67 were studied by flow cytometry in inguinal LN biopsies. Control and KMOi-treated animals showed different patterns of T cell activation. PD-1 expression in CD4+ T cells (Fig. 4A) rose during acute SIV infection to peak at 12 weeks p.i. before gradually diminishing, but this increase in PD-1 expression was blunted in the KMOi-treated animals, with significantly less expression at 12 weeks p.i. ($P < 0.05$). A trend towards lower PD-1 in the treated group was apparent up to 40 weeks p.i., even though dosing of KMOi ceased at 4 weeks p.i. Lower Ki67 expression in the treated group was also evident at 8 weeks p.i. (Fig. 4A), with a similar pattern observed for CD8+ T cells (Fig. 4B).

In PBMCs, significantly lower levels of PD-1 expression were also evident, in addition to lower expression of HLA-DR and Ki67 in both CD4+ and CD8+ T cells (Supplemental Fig. 1). Analysis of other parameters of immune phenotype and function showed no difference between the KMOi-treated and control groups. No differences between groups were noted in levels of IP-10, TNFRα1, and sCD14 soluble markers of immune activation from plasma (data not shown). Since the checkpoint inhibitor PD-1 is upregulated on exhausted T cells (8, 41), and blockade of this molecule can increase T cell functionality (41–44), bulk CD4+ and CD8+ T cells were assessed by CFC to determine whether KMO inhibition increased polyfunctional or SIV-specific IFNα, TNFα, IL-2 or IL-17 production above that in control animals, however, this was not observed (Supplemental Fig. 4 and data not shown).

KMO inhibition increases naïve T cell frequency in SIV-infected animals

To evaluate whether KMO inhibition modified the proportions of naïve and memory cells, T cell expression of CD95 and CD28 was determined by flow cytometry from cells isolated from inguinal LN. Naïve T cells were defined as CD95-CD28+, central memory (CM) T cells as CD95+CD28+, and effector memory (EM) T cells as CD95+CD28-. Higher frequencies of naïve cells were present in both CD4+ (Fig. 5A) and CD8+ T cells (Fig. 5B) in KMOi-treated animals, manifesting at 8 weeks p.i. when these differences were

statistically significant ($P < 0.05$), and sustained at higher levels than those seen in controls until 40 weeks p.i. These higher proportions of naïve T cells were counterbalanced by lower frequencies of CM cells, while proportions of EM were similar between groups in both CD4+ and CD8+ T cells. While the difference between treatment groups was not as striking as that seen in LN, higher proportions of naïve and lower proportions of CM T cells was also evident in both CD4+ and CD8+ PBMC T cells (Supplemental Fig. 2).

We hypothesized that the increased proportions of naïve T cells may be due to greater thymic function or thymocyte survival in the presence of KMOi, as downstream KP metabolites can induce thymocyte apoptosis (45). Since cryopreserved cells were not available to measure thymic output by T cell receptor excision circles (46), we instead evaluated the activity of KMOi CHDI-340246 in SCID-hu Thy/Liv mice inoculated with HIV-1 NL4–3. No significant differences were observed in thymic cellularity, CD4/CD8 frequencies, or VL (data not shown), suggesting either that mechanisms unrelated to thymic function or thymocyte survival may have resulted in the observed modified proportions of naïve/memory cells in the KMOi-treated rhesus macaques, or that such mechanisms were not revealed in the SCID-hu experiments that we performed.

KMO inhibition lowers PD-1 expression within naïve and memory T cell subsets of SIV-infected animals

PD-1 is expressed on a greater frequency of memory cells than naïve cells (47, 48). To determine whether the higher proportion of naive cells in the KMOi-treated animals (Fig. 5) explained the lower frequency of PD-1 expression (Fig. 4), PD-1 expression was analyzed within the naïve, CM, and EM CD4+ and CD8+ T cell subsets of LN (Fig. 6). Although in the absence of HIV/SIV infection, naïve T cells express negligible PD-1, HIV/SIV infection induces PD-1 expression on a fraction of naïve T cells (48). This was also observed in our study, with >10% of CD4+ naïve T cells and >20% of CD8+ naïve T cells in the control group expressing PD-1 at 8 weeks p.i. Significantly fewer naïve and CM CD4+ T cells from KMOi-treated animals expressed PD-1 at 12 weeks p.i., and there was a trend for lower frequencies of PD-1 expression within all CD8+ T cell subsets. These data indicate that lower proportions of PD-1-expressing cells on bulk T cells were not merely the result of the KMOi modifying proportions of naïve and memory T cells; indeed, PD-1 expression was intrinsically lower within both naïve and memory populations. In addition, the PD-1 MFI was lower in the KMOi treated animals in total, naïve, central memory, and effector memory gated PD-1+ populations (Supplemental Fig. 3).

Early PD-1 expression during acute SIV infection predicts clinical outcomes of body weight and CD4+ T cell counts

A striking feature of the clinical outcomes of KMO inhibition shown in Figs. 2A and 2B is that the differences between treatment groups only became apparent after cART initiation, and reached statistical significance 6 months p.i., even though KMOi was only administered for the first 4 weeks of the study. By contrast, immunological outcomes (reduced PD-1 expression and increased naïve T cell frequencies), (Figs. 4–6), were evident either at the end of the dosing phase or shortly thereafter. To determine whether early PD-1 expression in acute infection predicted clinical outcomes of body weight and CD4+ T cell counts later in

the study, we performed linear regressions between the frequency of PD-1+ T cells at −2, 4, and 8 weeks p.i. and the outcome variables of body weight (Fig. 7A) and CD4+ T cell counts (Fig. 7B) at 48 weeks p.i.

For body weight at 48 weeks p.i., significant ($P < 0.05$) negative relationships were found for PD-1 expression at week 8 in CD4+ T cells and at week 4 in CD8+ T cells (Fig. 7B). Similar data were observed when expression of PD-1 was assessed as a predictor of outcome CD4+ T cell counts (Fig. 7B). However, no correlation was observed between PD-1 expression at pre-infection baseline and either clinical outcome at 48 weeks p.i., suggesting that modulation of PD-1 by KMOi may be predictive of slower disease progression.

To determine if retention of Th17 cells may be a potential mechanism for the beneficial actions of KMOi in this study, IL-17+ CD4+ T cells were measured by CFC. The frequency of IL-17+ CD4+ T cells dropped during acute infection in both groups, and then gradually recovered after 6 weeks p.i, as expected. As the frequency increased, however, the % of CD4+ cells expressing IL-17 in KMOi-treated animals never reached the IL-17 frequencies detected in control animals (Supplemental Fig. 4A). IHC staining of IL-17 was performed in inguinal LN and RB gut samples to determine whether Th17 levels in tissues may have been modulated by KMOi. No significant differences were observed between treatment groups (Supplemental Fig. 4B and 4C). To evaluate whether microbial translocation may have played a role in the effects of KMO inhibition independent of IL-17, we measured proxies for microbial translocation: sCD14 in plasma by ELISA and neutrophil infiltration in RB by myeloperoxidase (MPO) IHC staining. Both analytes initially increased during acute SIV infection, but measurements out to 12 weeks p.i. indicated no differences between treatment groups (data not shown).

During HIV/SIV infection, Treg recruited into lymphoid tissues produce TGFβ (49), inducing fibroblasts to produce collagen that eventually replaces the fibroblastic reticular cell network (FRCn); this results in the loss of the important T cell survival cytokine IL-7 (49–51) and leads to naïve T cell depletion (52). To investigate whether KMOi inhibited these processes, collagen deposition and TGFβ expression were analyzed in LN by IHC staining, Treg frequencies were monitored by flow cytometry, and IL-7 levels were measured in plasma by ELISA. No significant differences in any of these parameters were observed between treatment groups (data not shown).

Discussion

These data demonstrate that inhibition of KMO in acute SIV infection disrupts the KP and prevents SIV-induced increases in downstream metabolites, with the resultant effect of improving clinical outcome as measured by both increased CD4+ T cell counts and body weight. Although the mechanisms driving this finding are unknown, it is possible that transient KMO inhibition had a durable impact on long-lived cells (or entrenched an important *process*) important for weight gain. KMO inhibition lowered T cell PD-1 expression and increased naïve T cell frequency in SIV-infected animals; of note, KMO inhibition lowered PD-1 expression even within naïve and memory T cell subsets. Importantly, early PD-1 expression during acute SIV infection predicted clinical outcomes

of body weight and CD4+ T cell counts, suggesting a causal relationship between the KMOi-driven PD-1 decrease and clinical outcome.

The PD-1 pathway has been implicated in the exhaustion of virus-specific T cells during chonic HIV infection (7, 47, 48) and PD-1 blockade is being investigated as an intervention therapy in HIV/SIV infection. A humanized mouse model found improved CD4+ T cell counts with PD-1 blockade (42), consistent with our finding of a significant relationship between reduced PD-1 expression and improvement in CD4+ T cell counts. In some humanized mice and non-human primate studies, PD-1 blockade has resulted in enhanced HIV/SIV-specific responses and a decrease in plasma VL (42–44). Despite the reduced PD-1 expression on both CD4+ and CD8+ T cells in KMOi-treated animals, we did not find evidence of increased antigen specific or polyclonal cytokine responses, even when normalized for the proportions of memory cells (Supplemental Fig. 4 and data not shown), nor was there a difference in VL between treatment groups. The link between the impact of PD-1 blockade on SIV-specific T cell responses and VL is uncertain, however, as some studies have shown limited therapeutic benefit of PD-1 blockade during chonic SIV infection, despite enhanced SIV-specific T cell responses (53, 54).

A number of key questions remain to be addressed. Although we have shown that KMO inhibition lowered PD-1 expression and increased naïve T cell frequencies, we do not know the mechanism(s) by which this occurred. Interestingly, a recent publication reported that KYN exposure directly upregulated PD-1 expression in CD8+ T cells via AhR activation (55), opposite to the repression of PD-1 we observed in the presence of KMOi mediated higher KYN concentrations. The reasons for this discrepancy are unknown, but Chen *et al* note that for maximal effect, TCR priming was required, whereas TCR signaling would have been largely absent in our study.

The increased frequencies of naïve T cells could result from improved thymic function, differential rates of thymocyte/naïve/memory T cell survival and proliferation, and/or alterations in the differentiation rate from naïve to CM. Although we found no evidence of KMO inhibition on thymic functionality in SCID-hu Thy/Liv mice inoculated with HIV-1, these studies were not definitive. Given recent evidence that exogenous KYN treatment leads to a dose-dependent inhibition of IL-2 signaling in memory CD4+ T cells, thereby inhibiting memory T cell survival and cytokine induced proliferation (56), future experiments might examine the proliferative capacity of naïve and memory T cell subsets *ex vivo*. No differences were observed in collagen deposition and TGFβ expression in LN, Treg frequencies, and plasma IL-7 levels, suggesting that enhanced preservation of LN fibroblastic reticular cell network in KMOi-treated animals is unlikely the cause of increased naïve T cell frequencies. Although Tregs may be expected to increase in the presence of KMOi due to the build up of KYN which induces AhR, (18), the resultant decrease in the downstream metabolite 3-HAA could cause a reduction in Treg (57). The engagement of two opposing mechanisms may explain the lack of significant changes in Treg frequencies.

It is notable that, in our proof of concept study, distinctions in clinical outcome between the treatment groups only became apparent months after cART initiation, even though KMOi was administered for just the first 4 weeks of the study. This demonstrates that changes

which occur at the outset of infection can have profound effects at later timepoints. Most HIV-infected individuals initially present to the clinic many weeks to even years after infection and are soon thereafter put on cART, long after the window of very early KMOi treatment tested in our study. Based on our findings of KMO inhibition during acute SIV infection, we wonder whether KMO inhibition might also provide benefit in the setting of chonic cART-treated infection, where immune activation has been shown to persist.

The KP has also been implicated in the pathogenesis of HIV-associated neurocognitive disorder (HAND) (20, 27). It would thus also be of interest to evaluate KMO inhibition in the context of HIV dementia models, or other models of neuroinflammation that lead to an upregulation of the KP pathway, as CHDI-340246 can modulate the KP in the primate central nervous system (IMS, personal communication). Together, these data provide a rationale for testing the KMOi, CHDI-340246, as adjunctive treatment in SIV/HIV infection to slow progression of disease and to improve immune reconstitution.

Supplementary Material

Refer to Web version on PubMed Central for supplementary material.

Acknowledgments

We are grateful to Gilead for kindly providing tenofovir and emtricitabine, and to ViiV for the provision of dolutegravir for cART treatment.

We thank CHDI Foundation for its support of this study and providing the KMO inhibitor, CHDI-340246. Additional funding was provided by DARE (Delaney AIDS Research Enterprise to Defeat HIV) and the ONPRC NIH grant award P51OD011092, and with federal funds from the NCI, under Contract No. HHSN261200800001E. The content of this publication does not necessarily reflect the views or policies of the Department of Health and Human Services (DHHS), nor does the mention of trade names, commercial products, or organizations imply endorsement by the U.S. Government.

References

1. Hazenberg MD, Hamann D, Schuitemaker H, and Miedema F 2000 T cell depletion in HIV-1 infection: how CD4+ T cells go out of stock. Nature Immunology 1: 285 EP–289. [PubMed: 11017098]
2. McCune JM 2001 The dynamics of CD4+ T-cell depletion in HIV disease. Nature 2006 443:7109 410: 974 EP–979.
3. Grossman Z, Meier-Schellersheim M, Sousa AE, Victorino RMM, and Paul WE 2002 CD4+ T-cell depletion in HIV infection: are we closer to understanding the cause? Nat Med 8: 319–323. [PubMed: 11927927]
4. Douek DC, Picker LJ, and Koup RA 2003 T cell dynamics in HIV-1 infection. Annu. Rev. Immunol 21: 265–304. [PubMed: 12524385]
5. Tenorio AR, Zheng Y, Bosch RJ, Krishnan S, Rodriguez B, Hunt PW, Plants J, Seth A, Wilson CC, Deeks SG, Lederman MM, and Landay AL 2014 Soluble markers of inflammation and coagulation but not T-cell activation predict non-AIDS-defining morbid events during suppressive antiretroviral treatment. J. Infect. Dis 210: 1248–1259. [PubMed: 24795473]
6. Hunt PW, Sinclair E, Rodriguez B, Shive C, Clagett B, Funderburg N, Robinson J, Huang Y, Epling L, Martin JN, Deeks SG, Meinert CL, Van Natta ML, Jabs DA, and Lederman MM 2014 Gut epithelial barrier dysfunction and innate immune activation predict mortality in treated HIV infection. J. Infect. Dis 210: 1228–1238. [PubMed: 24755434]
7. Trautmann L, Janbazian L, Chomont N, Said EA, Gimmig S, Bessette B, Boulassel M-R, Delwart E, Sepulveda H, Balderas RS, Routy J-P, Haddad EK, and Sekaly R-P 2006 Upregulation of PD-1

expression on HIV-specific CD8+ T cells leads to reversible immune dysfunction. Nat Med 12: 1198–1202. [PubMed: 16917489]

8. Day CL, Kaufmann DE, Kiepiela P, Brown JA, Moodley ES, Reddy S, Mackey EW, Miller JD, Leslie AJ, DePierres C, Mncube Z, Duraiswamy J, Zhu B, Eichbaum Q, Altfeld M, Wherry EJ, Coovadia HM, Goulder PJR, Klenerman P, Ahmed R, Freeman GJ, and Walker BD 2006 PD-1 expression on HIV-specific T cells is associated with T-cell exhaustion and disease progression. Nature 2006 443:7109 443: 350–354.
9. Favre D, Lederer S, Kanwar B, Ma Z-M, Proll S, Kasakow Z, Mold J, Swainson L, Barbour JD, Baskin CR, Palermo R, Pandrea I, Miller CJ, Katze MG, and McCune JM 2009 Critical loss of the balance between Th17 and T regulatory cell populations in pathogenic SIV infection. PLoS Pathog. 5: e1000295. [PubMed: 19214220]
10. Favre D, Mold J, Hunt PW, Kanwar B, Loke P, Seu L, Barbour JD, Lowe MM, Jayawardene A, Aweeka F, Huang Y, Douek DC, Brenchley JM, Martin JN, Hecht FM, Deeks SG, and McCune JM 2010 Tryptophan catabolism by indoleamine 2,3-dioxygenase 1 alters the balance of TH17 to regulatory T cells in HIV disease. Sci Transl Med 2: 32ra36–32ra36.
11. Routy J-P, Mehraj V, Vyboh K, Cao W, Kema I, and Jenabian M-A 2015 Clinical Relevance of Kynurenine Pathway in HIV/AIDS: An Immune Checkpoint at the Crossroads of Metabolism and Inflammation. AIDS Rev 17: 96–106. [PubMed: 26035167]
12. Cantó C, Menzies KJ, and Auwerx J 2015 NAD(+) Metabolism and the Control of Energy Homeostasis: A Balancing Act between Mitochondria and the Nucleus. Cell Metab 22: 31–53. [PubMed: 26118927]
13. Cervenka I, Agudelo LZ, and Ruas JL 2017 Kynurenines: Tryptophan's metabolites in exercise, inflammation, and mental health. Science 357: eaaf9794. [PubMed: 28751584]
14. Strasser B, Becker K, Fuchs D, and Gostner JM 2017 Kynurenine pathway metabolism and immune activation: Peripheral measurements in psychiatric and co-morbid conditions. Neuropharmacology 112: 286–296. [PubMed: 26924709]
15. Schmidt SV, and Schultze JL 2014 New Insights into IDO Biology in Bacterial and Viral Infections. Front. Immunol 5: 384. [PubMed: 25157255]
16. Godin-Ethier J, Hanafi L-A, Piccirillo CA, and Lapointe R 2011 Indoleamine 2,3-dioxygenase expression in human cancers: clinical and immunologic perspectives. Clin. Cancer Res 17: 6985–6991. [PubMed: 22068654]
17. Chung DJ, Rossi M, Romano E, Ghith J, Yuan J, Munn DH, and Young JW 2009 Indoleamine 2,3-dioxygenase-expressing mature human monocyte-derived dendritic cells expand potent autologous regulatory T cells. Blood 114: 555–563. [PubMed: 19465693]
18. Mezrich JD, Fechner JH, Zhang X, Johnson BP, Burlingham WJ, and Bradfield CA 2010 An interaction between kynurenine and the aryl hydrocarbon receptor can generate regulatory T cells. J. Immunol 185: 3190–3198. [PubMed: 20720200]
19. Frumento G, Rotondo R, Tonetti M, Damonte G, Benatti U, and Ferrara GB 2002 Tryptophan-derived catabolites are responsible for inhibition of T and natural killer cell proliferation induced by indoleamine 2,3-dioxygenase. J. Exp. Med 196: 459–468. [PubMed: 12186838]
20. Guillemin GJ, Wang L, and Brew BJ 2005 Quinolinic acid selectively induces apoptosis of human astrocytes: potential role in AIDS dementia complex. J Neuroinflammation 2: 16. [PubMed: 16042813]
21. Vujkovic-Cvijin I, Swainson LA, Chu SN, Ortiz AM, Santee CA, Petriello A, Dunham RM, Fadrosh DW, Lin DL, Faruqi AA, Huang Y, Apetrei C, Pandrea I, Hecht FM, Pilcher CD, Klatt NR, Brenchley JM, Lynch SV, and McCune JM 2015 Gut-Resident Lactobacillus Abundance Associates with IDO1 Inhibition and Th17 Dynamics in SIV-Infected Macaques. CellReports 13: 1589–1597.
22. Jenabian M-A, Patel M, Kema I, Kanagaratham C, Radzioch D, Thébault P, Lapointe R, Tremblay C, Gilmore N, Ancuta P, and Routy J-P 2013 Distinct tryptophan catabolism and Th17/Treg balance in HIV progressors and elite controllers. PLoS ONE 8: e78146. [PubMed: 24147117]
23. Stephens GL, Wang Q, Swerdlow B, Bhat G, Kolbeck R, and Fung M 2013 Kynurenine 3-monooxygenase mediates inhibition of Th17 differentiation via catabolism of endogenous aryl hydrocarbon receptor ligands. Eur. J. Immunol 43: 1727–1734. [PubMed: 23568529]

24. Hunt PW 2010 Th17, gut, and HIV: therapeutic implications. Curr Opin HIV AIDS 5: 189–193. [PubMed: 20543599]
25. Byakwaga H, Boum Y, Huang Y, Muzoora C, Kembabazi A, Weiser SD, Bennett J, Cao H, Haberer JE, Deeks SG, Bangsberg DR, McCune JM, Martin JN, and Hunt PW 2014 The kynurenine pathway of tryptophan catabolism, CD4+ T-cell recovery, and mortality among HIV-infected Ugandans initiating antiretroviral therapy. J. Infect. Dis 210: 383–391. [PubMed: 24585899]
26. Lee S, Byakwaga H, Boum Y, Burdo TH, Williams KC, Lederman MM, Huang Y, Tracy RP, Cao H, Haberer JE, Kembabazi A, Bangsberg DR, Martin JN, and Hunt PW 2017 Immunologic Pathways That Predict Mortality in HIV-Infected Ugandans Initiating Antiretroviral Therapy. J. Infect. Dis 215: 1270–1274. [PubMed: 28329310]
27. Heyes MP, Brew BJ, Martin A, Price RW, Salazar AM, Sidtis JJ, Yergey JA, Mouradian MM, Sadler AE, and Keilp J 1991 Quinolinic acid in cerebrospinal fluid and serum in HIV-1 infection: relationship to clinical and neurological status. Ann Neurol 29: 202–209. [PubMed: 1826418]
28. Giorgini F, Guidetti P, Nguyen Q, Bennett SC, and Muchowski PJ 2005 A genomic screen in yeast implicates kynurenine 3-monooxygenase as a therapeutic target for Huntington disease. Nat Genet 37: 526–531. [PubMed: 15806102]
29. Thevandavakkam MA, Schwarcz R, Muchowski PJ, and Giorgini F 2010 Targeting kynurenine 3-monooxygenase (KMO): implications for therapy in Huntington's disease. CNS Neurol Disord Drug Targets 9: 791–800. [PubMed: 20942784]
30. Beaumont V, Mrzljak L, Dijkman U, Freije R, Heins M, Rassoulpour A, Tombaugh G, Gelman S, Bradaia A, Steidl E, Gleyzes M, Heikkinen T, Lehtimäki K, Puoliväli J, Kontkanen O, Javier RM, Neagoe I, Deisemann H, Winkler D, Ebneth A, Khetarpal V, Toledo-Sherman L, Dominguez C, Park LC, and Munoz-Sanjuan I 2016 The novel KMO inhibitor CHDI-340246 leads to a restoration of electrophysiological alterations in mouse models of Huntington's disease. Exp. Neurol 282: 99–118. [PubMed: 27163548]
31. Zwilling D, Huang S-Y, Sathyasaikumar KV, Notarangelo FM, Guidetti P, Wu H-Q, Lee J, Truong J, Andrews-Zwilling Y, Hsieh EW, Louie JY, Wu T, Scearce-Levie K, Patrick C, Adame A, Giorgini F, Moussaoui S, Laue G, Rassoulpour A, Flik G, Huang Y, Muchowski JM, Masliah E, Schwarcz R, and Muchowski PJ 2011 Kynurenine 3-monooxygenase inhibition in blood ameliorates neurodegeneration. Cell 145: 863–874. [PubMed: 21640374]
32. Favennec M, Hennart B, Caiazzo R, Leloire A, Yengo L, Verbanck M, Arredouani A, Marre M, Pigeyre M, Bessede A, Guillemin GJ, Chinetti G, Staels B, Pattou F, Balkau B, Allorge D, Froguel P, and Poulain-Godefroy O 2015 The kynurenine pathway is activated in human obesity and shifted toward kynurenine monooxygenase activation. Obesity (Silver Spring) 23: 2066–2074. [PubMed: 26347385]
33. Connor TJ, Starr N, O'Sullivan JB, and Harkin A 2008 Induction of indolamine 2,3-dioxygenase and kynurenine 3-monooxygenase in rat brain following a systemic inflammatory challenge: a role for IFN-gamma? Neurosci. Lett 441: 29–34. [PubMed: 18584961]
34. Baker CAR, Swainson L, Lin DL, Wong S, Hartigan-O'Connor DJ, Lifson JD, Tarantal AF, and McCune JM 2015 Exposure to SIV in utero results in reduced viral loads and altered responsiveness to postnatal challenge. Sci Transl Med 7: 300ra125–300ra125.
35. Estes JD, Kityo C, Ssali F, Swainson L, Makamdop KN, Del Prete GQ, Deeks SG, Luciw PA, Chipman JG, Beilman GJ, Hoskuldsson T, Khoruts A, Anderson J, Deleage C, Jasurda J, Schmidt TE, Hafertepe M, Callisto SP, Pearson H, Reimann T, Schuster J, Schoephoerster J, Southern P, Perkey K, Shang L, Wietgrefe SW, Fletcher CV, Lifson JD, Douek DC, McCune JM, Haase AT, and Schacker TW 2017 Defining total-body AIDS-virus burden with implications for curative strategies. Nat. Med 23: 1271–1276. [PubMed: 28967921]
36. Deleage C, Wietgrefe SW, Del Prete G, Morcock DR, Hao XP, Piatak M, Bess J, Anderson JL, Perkey KE, Reilly C, McCune JM, Haase AT, Lifson JD, Schacker TW, and Estes JD 2016 Defining HIV and SIV Reservoirs in Lymphoid Tissues. Pathog Immun 1: 68–106. [PubMed: 27430032]
37. Deleage C, Schuetz A, Alvord WG, Johnston L, Hao XP, Morcock DR, Rerknimitr R, Fletcher JLK, Puttamaswin S, Phanuphak N, Dewar R, McCune JM, Sereti I, Robb M, Kim JH, Schacker

TW, Hunt P, Lifson JD, Ananworanich J, and Estes JD 2016 Impact of early cART in the gut during acute HIV infection. JCI Insight 1: 1365.

38. Somsouk M, Estes JD, Deleage C, Dunham RM, Albright R, Inadomi JM, Martin JN, Deeks SG, McCune JM, and Hunt PW 2015 Gut epithelial barrier and systemic inflammation during chronic HIV infection. AIDS 29: 43–51. [PubMed: 25387317]
39. Tabb B, Morcock DR, Trubey CM, Quiñones OA, Hao XP, Smedley J, Macallister R, Piatak M, Harris LD, Paiardini M, Silvestri G, Brenchley JM, Alvord WG, Lifson JD, and Estes JD 2013 Reduced inflammation and lymphoid tissue immunopathology in rhesus macaques receiving anti-tumor necrosis factor treatment during primary simian immunodeficiency virus infection. J. Infect. Dis 207: 880–892. [PubMed: 23087435]
40. Toledo-Sherman LM, Prime ME, Mrzljak L, Beconi MG, Beresford A, Brookfield FA, Brown CJ, Cardaun I, Courtney SM, Dijkman U, Hamelin-Flegg E, Johnson PD, Kempf V, Lyons K, Matthews K, Mitchell WL, O'Connell C, Pena P, Powell K, Rassoulpour A, Reed L, Reindl W, Selvaratnam S, Friley WW, Weddell DA, Went NE, Wheelan P, Winkler C, Winkler D, Wityak J, Yarnold CJ, Yates D, Munoz-Sanjuan I, and Dominguez C 2015 Development of a Series of Aryl Pyrimidine Kynurenine Monooxygenase Inhibitors as Potential Therapeutic Agents for the Treatment of Huntington's Disease. J. Med. Chem 58: 1159–1183. [PubMed: 25590515]
41. Barber DL, Wherry EJ, Masopust D, Zhu B, Allison JP, Sharpe AH, Freeman GJ, and Ahmed R 2006 Restoring function in exhausted CD8 T cells during chronic viral infection. Nature 2006 443:7109 439: 682–687.
42. Palmer BE, Neff CP, Lecureux J, Ehler A, Dsouza M, Remling-Mulder L, Korman AJ, Fontenot AP, and Akkina R 2013 In vivo blockade of the PD-1 receptor suppresses HIV-1 viral loads and improves CD4+ T cell levels in humanized mice. J. Immunol 190: 211–219. [PubMed: 23209326]
43. Seung E, Dudek TE, Allen TM, Freeman GJ, Luster AD, and Tager AM 2013 PD-1 blockade in chronically HIV-1-infected humanized mice suppresses viral loads. PLoS ONE 8: e77780. [PubMed: 24204962]
44. Velu V, Titanji K, Zhu B, Husain S, Pladevega A, Lai L, Vanderford TH, Chennareddi L, Silvestri G, Freeman GJ, Ahmed R, and Amara RR 2009 Enhancing SIV-specific immunity in vivo by PD-1 blockade. Nature 2006 443:7109 458: 206–210.
45. Hiramatsu R, Hara T, Akimoto H, Takikawa O, Kawabe T, Isobe K-I, and Nagase F 2008 Cinnabarinic acid generated from 3-hydroxyanthranilic acid strongly induces apoptosis in thymocytes through the generation of reactive oxygen species and the induction of caspase. J. Cell. Biochem 103: 42–53. [PubMed: 17476692]
46. Harris JM, Hazenberg MD, Poulin J-F, Higuera-Alhino D, Schmidt D, Gotway M, and McCune JM 2005 Multiparameter evaluation of human thymic function: interpretations and caveats. Clin. Immunol 115: 138–146. [PubMed: 15885636]
47. Petrovas C, Casazza JP, Brenchley JM, Price DA, Gostick E, Adams WC, Precopio ML, Schacker T, Roederer M, Douek DC, and Koup RA 2006 PD-1 is a regulator of virus-specific CD8+ T cell survival in HIV infection. J. Exp. Med 203: 2281–2292. [PubMed: 16954372]
48. Breton G, Chomont N, Takata H, Fromentin R, Ahlers J, Filali-Mouhim A, Riou C, Boulassel M-R, Routy J-P, Yassine-Diab B, and Sekaly R-P 2013 Programmed death-1 is a marker for abnormal distribution of naive/memory T cell subsets in HIV-1 infection. J. Immunol 191: 2194–2204. [PubMed: 23918986]
49. Estes JD, Li Q, Reynolds MR, Wietgrefe S, Duan L, Schacker T, Picker LJ, Watkins DI, Lifson JD, Reilly C, Carlis J, and Haase AT 2006 Premature induction of an immunosuppressive regulatory T cell response during acute simian immunodeficiency virus infection. J. Infect. Dis 193: 703–712. [PubMed: 16453267]
50. Estes JD, Wietgrefe S, Schacker T, Southern P, Beilman G, Reilly C, Milush JM, Lifson JD, Sodora DL, Carlis JV, and Haase AT 2007 Simian immunodeficiency virus-induced lymphatic tissue fibrosis is mediated by transforming growth factor beta 1-positive regulatory T cells and begins in early infection. J. Infect. Dis 195: 551–561. [PubMed: 17230415]
51. Zeng M, Smith AJ, Wietgrefe SW, Southern PJ, Schacker TW, Reilly CS, Estes JD, Burton GF, Silvestri G, Lifson JD, Carlis JV, and Haase AT 2011 Cumulative mechanisms of lymphoid tissue fibrosis and T cell depletion in HIV-1 and SIV infections. J. Clin. Invest 121: 998–1008. [PubMed: 21393864]

52. Estes JD, Gordon SN, Zeng M, Chahroudi AM, Dunham RM, Staprans SI, Reilly CS, Silvestri G, and Haase AT 2008 Early resolution of acute immune activation and induction of PD-1 in SIV-infected sooty mangabeys distinguishes nonpathogenic from pathogenic infection in rhesus macaques. J. Immunol 180: 6798–6807. [PubMed: 18453600]

53. Amancha PK, Hong JJ, Rogers K, Ansari AA, and Villinger F 2013 In vivo blockade of the programmed cell death-1 pathway using soluble recombinant PD-1-Fc enhances CD4+ and CD8+ T cell responses but has limited clinical benefit. J. Immunol. 191: 6060–6070. [PubMed: 24227774]

54. Finnefrock AC, Tang A, Li F, Freed DC, Feng M, Cox KS, Sykes KJ, Guare JP, Miller MD, Olsen DB, Hazuda DJ, Shiver JW, Casimiro DR, and Fu T-M 2009 PD-1 blockade in rhesus macaques: impact on chronic infection and prophylactic vaccination. J. Immunol 182: 980–987. [PubMed: 19124741]

55. Liu Y, Liang X, Dong W, Fang Y, Lv J, Zhang T, Fiskesund R, Xie J, Liu J, Yin X, Jin X, Chen D, Tang K, Ma J, Zhang H, Yu J, Yan J, Liang H, Mo S, Cheng F, Zhou Y, Zhang H, Wang J, Li J, Chen Y, Cui B, Hu Z-W, Cao X, Xiao-Feng Qin F, and Huang B 2018 Tumor-Repopulating Cells Induce PD-1 Expression in CD8+ T Cells by Transferring Kynurenine and AhR Activation. Cancer Cell 33: 480–494.e7. [PubMed: 29533786]

56. Dagenais-Lussier X, Aounallah M, Mehraj V, El-Far M, Tremblay C, Sekaly R-P, Routy J-P, and van Grevenynghe J 2016 Kynurenine Reduces Memory CD4 T-Cell Survival by Interfering with Interleukin-2 Signaling Early during HIV-1 Infection. J. Virol 90: 7967–7979. [PubMed: 27356894]

57. Yan Y, Zhang G-X, Gran B, Fallarino F, Yu S, Li H, Cullimore ML, Rostami A, and Xu H 2010 IDO upregulates regulatory T cells via tryptophan catabolite and suppresses encephalitogenic T cell responses in experimental autoimmune encephalomyelitis. J. Immunol 185: 5953–5961. [PubMed: 20944000]

Key Points

KMO inhibition improved clinical outcomes of CD4+ T cell counts and body weight

KMO inhibition increased naïve T cell frequency and lowered PD-1 expression

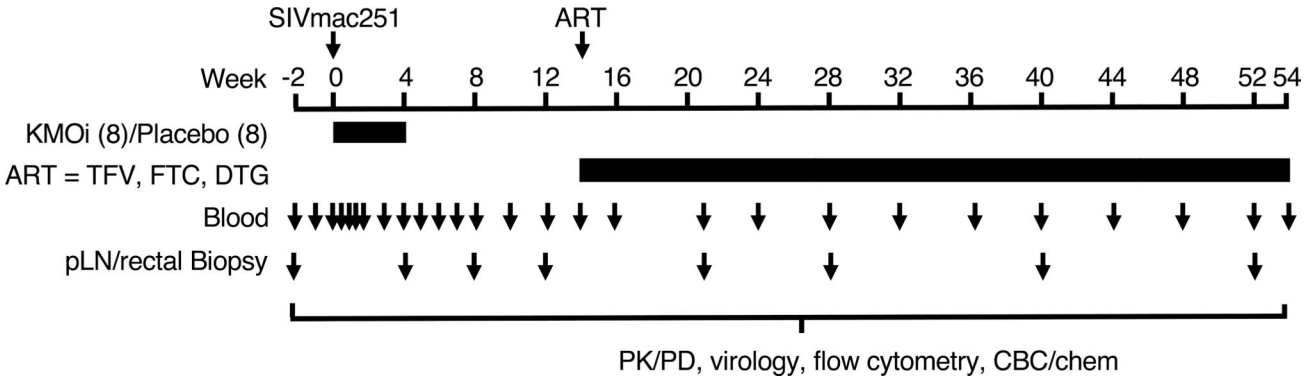

Figure 1. Study Design.

Timeline of treatment and sampling. Juvenile macaques were infected i.v. with SIVmac251 and treated for 4 weeks with KMOi CHDI-340246, or vehicle alone (8 animals per group). At 14 weeks post infection (p.i.), cART regimen was administered to all animals though the end of the study. Peripheral blood, peripheral LN, and RB were sampled at the indicated timepoints.

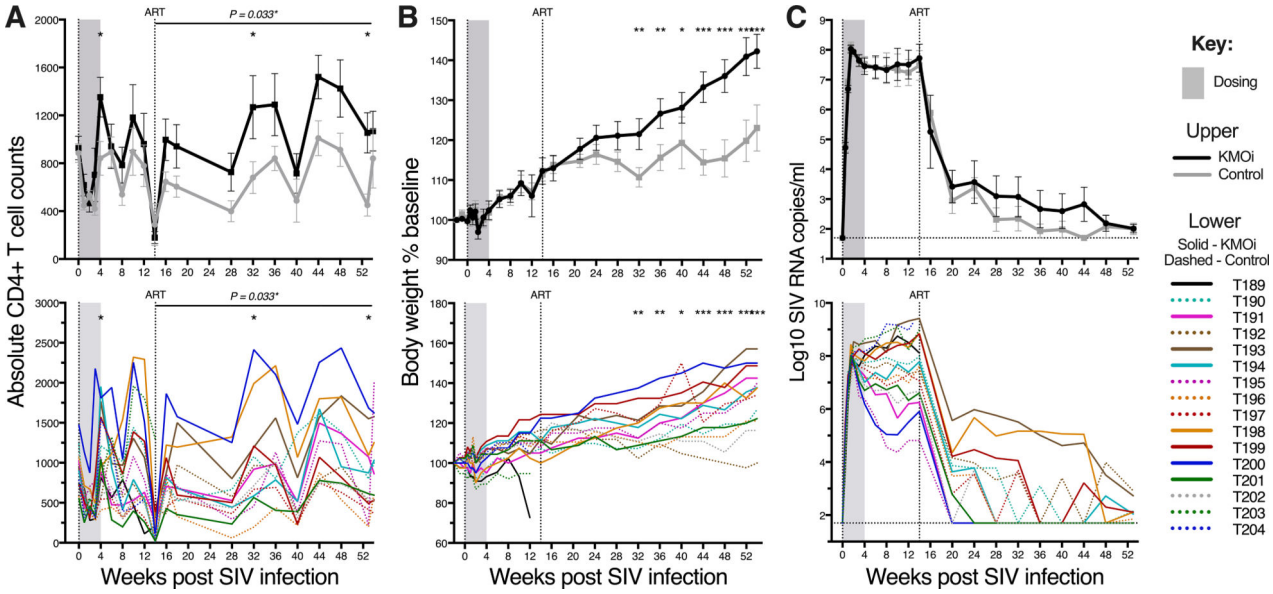

Figure 2. KMO inhibition increases CD4+ T cell counts and body weight in SIV-infected animals.

Graphs indicate clinical outcomes in KMOi-treated (black) and control animals (grey) with mean+/−SE (upper) and individual animals (lower). Grey shading indicates the dosing period and the vertical line shows cART initiation. (A) Y axis represents the circulating CD4+ T cell count. (B) Y axis represents body weight as a percentage of baseline. (C) Y axis represents log10 plasma SIV RNA VL. Horizontal line indicates sensitivity limit of assay (50 copies/ml). Differences between treatment groups in the change from baseline were assessed with linear mixed models.

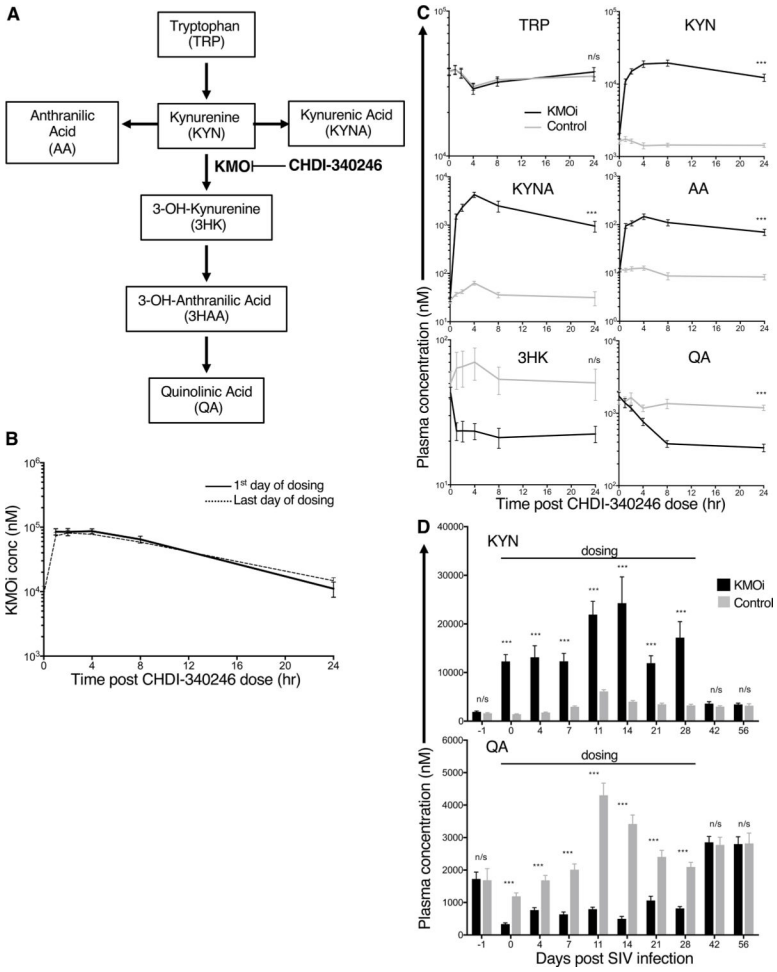

Figure 3. The KMOi CHDI-340246 disrupts the KP and prevents SIV-induced increases in downstream metabolites.

Concentrations of KMOi CHDI-340246 and KP metabolites were quantified in plasma by LC/MS/MS analysis. (A) The KP and point of KMO inhibition by CHDI-340246. (B) CHDI-340246 plasma concentrations during the 24 h after first and last dose. Mean +/− SEM of all treated animals is represented. (C) KP metabolite plasma concentrations during the 24 h after first dose. Mean +/− SEM of treated (black) and control animals (grey) is represented. Levels of 3HAA were low and in some cases below the limit of quantitation, and therefore considered unreliable to quantify. (D) Plasma concentrations of KYN (upper panel) and QA (lower panel) during the first 56 days after SIV infection. Mean + SEM of treated animals (black) and control animals (grey) is represented. Differences between treatment groups at indicated timepoints was assessed using Wilcoxon rank sum analysis.

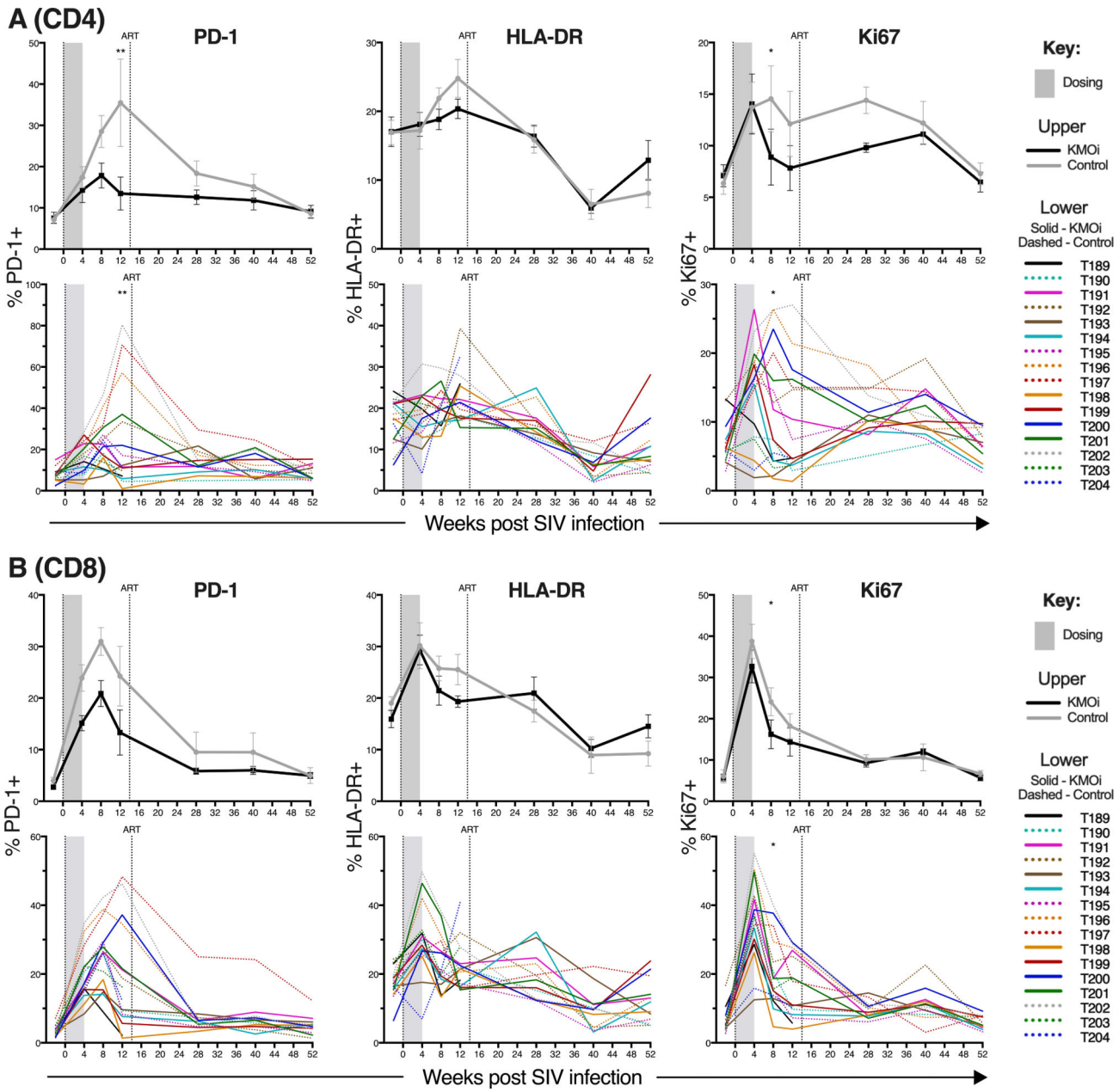

Figure 4. KMO inhibition lowers PD-1 expression in CD4+ and CD8+ T cells in SIV-infected animals.

Grey shading indicates the dosing period and the vertical line shows cART initiation. Graphs indicate % of CD4+ T cells (A) and CD8+ T cells (B) positive for the indicated activation markers in pLN as measured by flow cytometry. KMOi-treated (black) and control animals (grey) are represented with mean+/−SE shown in upper panels and individual animals in lower panels. Differences between treatment groups in the change from baseline were assessed with linear mixed models.

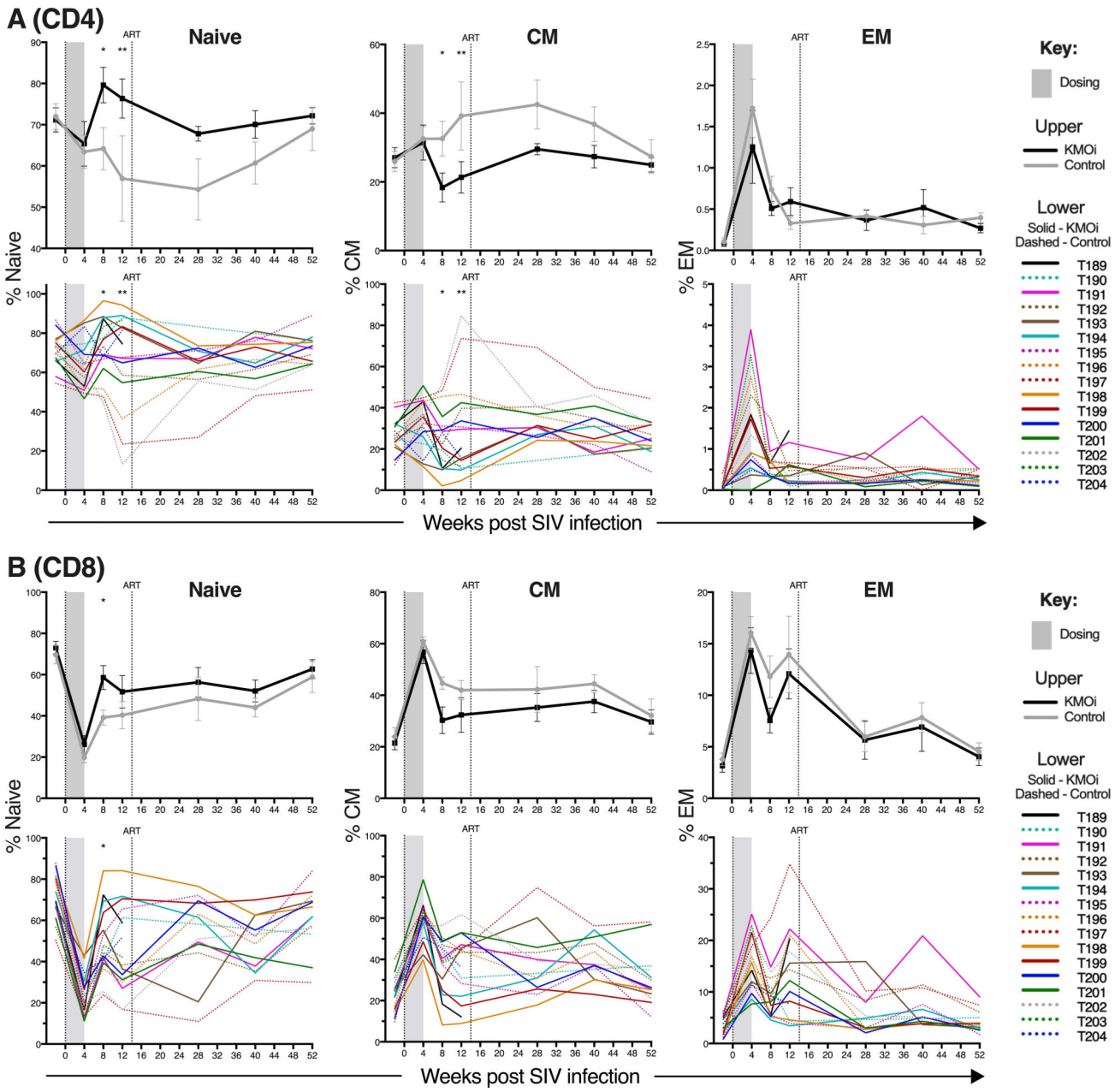

Figure 5. KMO inhibition increases naïve CD4+ and CD8+ T cell frequency in SIV-infected animals.

Grey shading indicates the dosing period and the vertical line shows cART initiation. Graphs indicate % of CD4+ T cells (A) and CD8+ T cells (B) identified as naïve, central memory (CM), or effector memory (EM) in pLN, as measured by flow cytometry. KMOi-treated (black) and control animals (grey) are represented with mean+/−SE shown in upper panels and individual animals in lower panels. Differences between treatment groups in the change from baseline were assessed with linear mixed models.

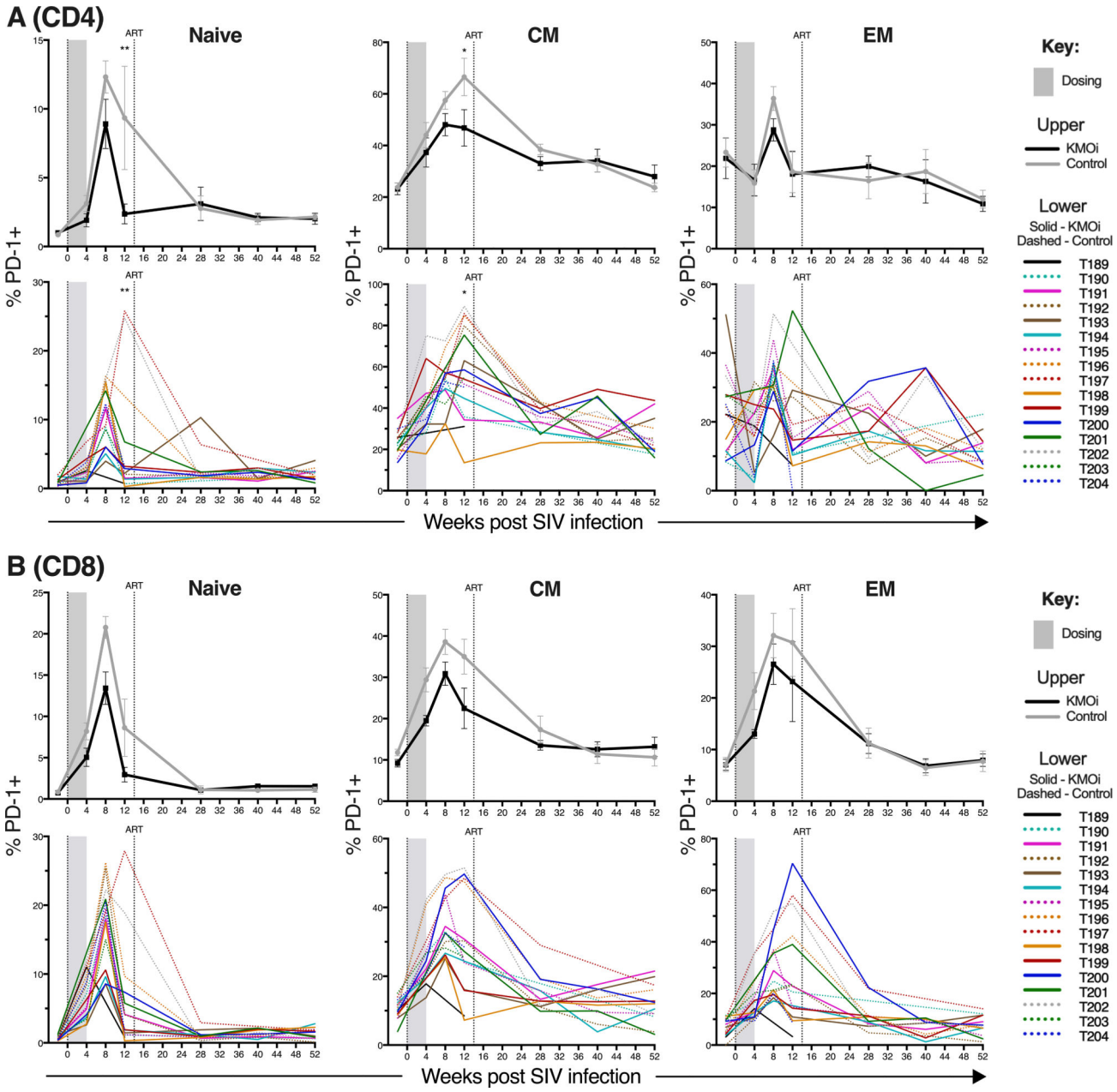

Figure 6. KMO inhibition lowers PD-1 expression within naïve and memory CD4+ and CD8+ T cell subsets in SIV-infected animals.

Grey shading indicates the dosing period and the vertical line shows cART initiation. Graphs indicate % of CD4+ T cells (A) and CD8+ T cells (B) positive for PD-1 within naïve, central memory (CM), or effector memory (EM) subsets in pLN, as measured by flow cytometry. KMOi-treated (black) and control animals (grey) are represented with mean+/−SE shown in upper panels and individual animals in lower panels. Differences between treatment groups in the change from baseline were assessed with linear mixed models.

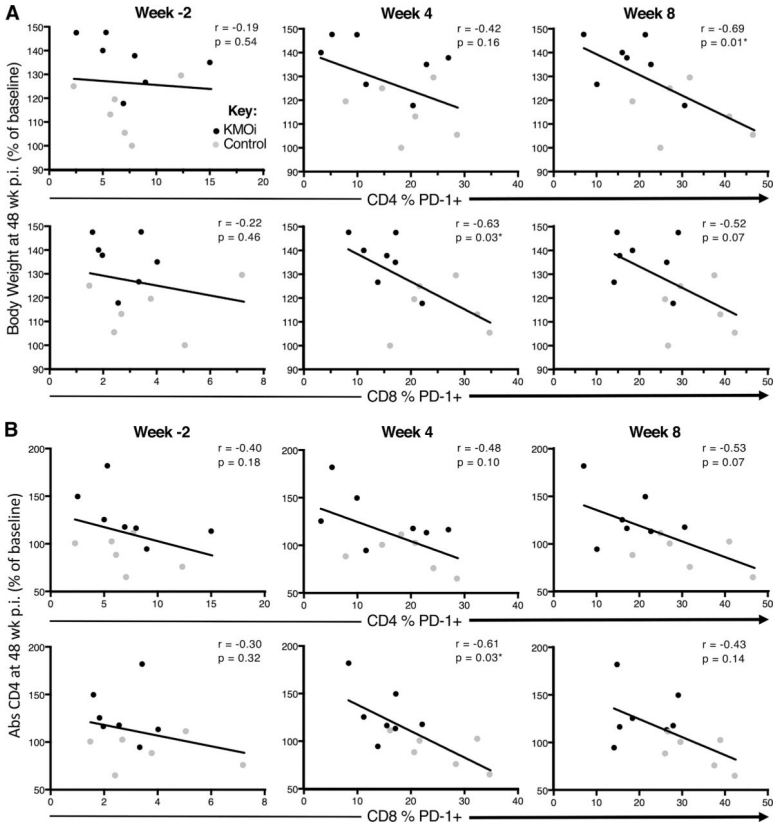

Figure 7. Early PD-1 expression during acute SIV infection predicts clinical outcomes of body weight and CD4+ T cell counts.

To investigate the impact of PD-1 expression pre- and post-treatment on subsequent clinical outcomes, linear regression was used to test for associations between the frequencies of PD-1+ T cells in CD4+ T cells (upper panels) and CD8+ T cells (lower panels) at timepoints −2 weeks (pre-treatment baseline), 4 weeks (end of treatment) and 8 weeks p.i. vs. the clinical outcome variables of body weight (A) and CD4+ T cell counts (B) at 48 weeks p.i. Spearman r and p values are indicated in each panel. KMOi-treated animals are indicated in black and control animals in grey.